# Tensile properties and microstructure of 2024 aluminum alloy subjected to the high magnetic field and external stress*

Gui-Rong Li(李桂荣)†, Fei Xue(薛飞), Hong-Ming Wang(王宏明), Rui Zheng(郑瑞), Yi Zhu(朱弋), Qiang-Ze Chu(储强泽), and Jiang-Feng Cheng(程江峰)

*School of Materials Science and Engineering, Jiangsu University, Zhenjiang* 212013, *China*

(Received 14 May 2016; revised manuscript received 28 June 2016; published online 25 August 2016)

In order to explore the dependence of plasticity of metallic material on a high magnetic field, the effects of the different magnetic induction intensities ($\boldsymbol{H} = 0$ T, 0.5 T, 1 T, 3 T, and 5 T) and pulses number ($N = 0$, 10, 20, 30, 40, and 50) on tensile strength ($\sigma_b$) and elongation ($\delta$) of 2024 aluminum alloy are investigated in the synchronous presences of a high magnetic field and external stress. The results show that the magnetic field exerts apparent and positive effects on the tensile properties of the alloy. Especially under the optimized condition of $\boldsymbol{H}^* = 1$ T and $N^* = 30$, the $\sigma_b$ and $\delta$ are 410 MPa and 17% that are enhanced by 9.3% and 30.8% respectively in comparison to those of the untreated sample. The synchronous increases of tensile properties are attributed to the magneto-plasticity effect on a quantum scale. That is, the magnetic field will accelerate the state conversion of radical pair generated between the dislocation and obstacles from singlet to the triplet state. The bonding energy between them is meanwhile lowered and the moving flexibility of dislocations will be enhanced. At $\boldsymbol{H}^* = 1$ T and $N^* = 30$, the dislocation density is enhanced by 1.28 times. The relevant minimum grain size is 266.1 nm, which is reduced by 35.2%. The grain refining is attributed to the dislocation accumulation and subsequent dynamic recrystallization. The (211) and (220) peak intensities are weakened. It is deduced that together with the recrystallization, the fine grains will transfer towards the slip plane and contribute to the slipping deformation.

**Keywords:** 2024 aluminum alloy, tensile strength, elongation, magneto plasticity effect

**PACS:** 62.20.–x, 81.40.Lm, 61.72.Lk **DOI:** 10.1088/1674-1056/25/10/106201

## 1. Introduction

The aluminum content in the Earth's crust accounts for about 8.3% of the total amount of the Earth's crust, which is only next to the oxygen and silicon element. In 1808, alumina was first electrolyzed into aluminum in the laboratory. When it joins other elements, the aluminum alloy will be synthesized. Nowadays various kinds of aluminum alloys are widely used in different fields. In all the available products the 2xxx and 7xxx series aluminum alloys have received more attention due to their excellent comprehensive performances.[1] Among the structural parts in the commercial aircraft, the usage of them has reached more than 80%. Besides this, these aluminum alloys are also widely utilized in the fields such as vehicle transport, weapons, electronic packaging, and so on.[2] The aluminum alloy of 2024 was invented in 1939, which exhibits high strength and good machinability, known as the duralumin. Till now, the 2024 aluminum alloy has been widely used in the aircraft structure such as (skin, frame, rib beam, frame, etc.), rivets, missile components, truck wheels, screw components and a variety of other structures. The proportion of utilized 2024 alloy is increased year by year in all aluminum alloys.[3] At present, the research of 2024 aluminum alloy focuses on a higher performance and lower cost. On the basis of a new design concept of aircraft, the demand for the structural part not only concentrates on the high strength but also superior plasticity and toughness, which has become an important task for materials scientists to meet the rigid requirement.

In recent years, with the technological development of physical fields, the electromagnetic fields have gradually been introduced into the material processing to improve the performance of metallic material.[4] Wang *et al.*[5] reported that the Lorenz force generated by a strong magnetic field can significantly inhibit convection in the melt, which affects the solidification behavior and microstructure remarkably. In 2012, Rao *et al.*[6] studied electrical and mechanical properties of a Cu–Cr–Zr alloy aged under an imposed DC current and static magnetic field, and the results indicated that the conductivity and micro hardness of the sample are significantly improved by the imposed electric-magnetic field. Katsuyuki *et al.*[7] studied the effect of plastic deformation on magnetic fields around fatigue crack tips of carbon tool steel (JIS,SKS93), and they found that the magnetic fields around the crack tip change during the crack growth, and also that the decrease in magnetic field depends on plastic deformation size. During the electromagnetic processing of materials, the fabricating conditions of materials would be affected obviously by an electromagnetic field, which covers the significant advantages, such as no change of the original ingredients, no pollution, no contact

*Project supported by the National Natural Science Foundation of China (Grant Nos. 51371091, 51174099, and 51001054) and the Industrial Center of Jiangsu University, China (Grant No. ZXJG201586).

†Corresponding author. E-mail: liguirong@ujs.edu.cn

© 2016 Chinese Physical Society and IOP Publishing Ltd 

with the sample, shortening the reaction time, enhancing the reaction efficiency, fining the grain size, etc. Among all the magnetic fields, the high pulsed electromagnetic field exhibited the force, heat and other peculiar effects on a quantum scale, which provides an innovative and potential way to improve the microstructure and strength, plasticity and toughness of metallic material.[8] Nevertheless, the available literature has rarely reported the influence of high pulsed magnetic field on the properties of solid aluminum alloy.

In this work, the 2024 aluminum alloy is selected as the research object. During the tensile test the high pulsed magnetic field is adopted to investigate its effect on the tensile properties, especially on the plasticity. The aim is not only to reveal the new effect of high magnetic field with different processing parameters, but also to explore an efficient approach to improving the strength, plasticity and toughness of conventional structural aluminum alloy. That is to say, on the assumption that the magnetic field takes a positive effect, it is expected to be introduced into the plastic deformation processes of metallic materials by squeezing and rolling them to enhance their productivities and mechanical properties.

## 2. Experimental procedures

### 2.1. Tensile experiment

The 2024 aluminum alloy subjected to squeezing, solution (510 °C ×40 min), aging treatment (120 °C ×24 h) was selected as the objects, whose main components detected by x-ray fluorescence spectrometer (XRF) are listed in Table 1.

**Table 1.** Major components of 2024 aluminum alloy (mass.%).

| Element | Al | Cu | Mg | Mn | Si | Fe | Zn | Cr |
|---|---|---|---|---|---|---|---|---|
| Amount | 94.97 | 3.04 | 0.553 | 0.515 | 0.381 | 0.275 | 0.162 | 0.0145 |

The magnetic field generator was mainly composed of pulses generator, solenoid coil and fixed clamp, pulse number recorder and the test samples bearing platform. The magnetic pulse was achieved through the discharging switch of the capacitor that was connected with the positive and negative electrodes of the coil. When the switch was on, the generator released a large pulsed current to the working coil, and then the pulsed magnetic field was produced in the chamber surrounded by the coil. Meanwhile the sample placed in the chamber would be subjected to the magnetic field treatment.

During the tensile test, the sample was exposed synchronously to the tensile stress and magnetic field generator. The main controlling parameters of the pulsed magnetic field were magnetic induction intensity ($\boldsymbol{H}$) and pulse number ($N$). Accordingly, the whole experiments were designed as two parts: (i) one focused on the influences of magnetic induction intensity on tensile property when the pulses number ($N$) was fixed at 30 and at $\boldsymbol{H} = 0$ T, 0.5 T, 1 T, 3 T, 5 T. On the basis of tested tensile properties, the suitable $\boldsymbol{H}^*$ was optimized; (ii) when $\boldsymbol{H} = \boldsymbol{H}^*$, the effects of pulse number were explored for $N = 10$, 20, 30, 40, 50 so as to acquire the optimal parameter of $N^*$. The total duration time of magnetic field was designed to be 600 s, the controlled interval times were 60 s, 30 s, 20 s, 15 s, and 12 s which correspond to the relevant 10, 20, 30, 40, 50 pulses, respectively.

Figure 1 illustrated the sample position in the magnetic field. In order to prevent the influence of strong force on the clamp due to high magnetic field, the specially designed clamp was different from the conventional ferromagnetic steel. They were made of nonmagnetic stainless steel together with extraordinary demand for the sample shape within the scope of the national standard. The tensile test was performed at room temperature. The 2024 aluminum alloy sample was fixed in the middle of solenoid coil, the inner of which was Φ5 mm and 50-mm height. The sample surface should be ensured to be parallel to the direction of magnetic induction lines.

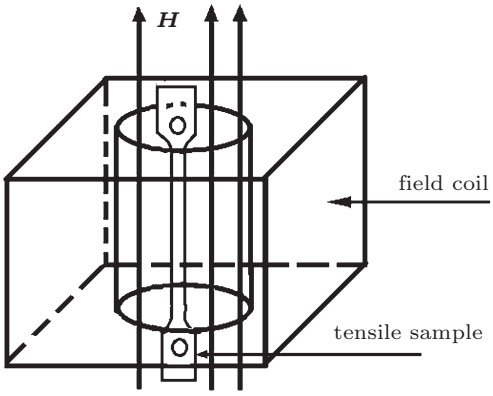



**Fig. 1.** Schematic diagram of sample position in the magnetic field.

The DWD-200 tensile machine was the main apparatus to measure the tensile properties. During the tensile test, the stretching rate was fixed at 1 mm/min. On this condition, it would take about 750 s for the sample from the stretch beginning to fracture.

The interval time $\Delta t$ between two adjacent pulses was dependent on $\boldsymbol{H}$. That was to say, the higher the $\boldsymbol{H}$, the longer the interval time would be. In fact, the interval time was just the charging process of the capacitor. For example, when $\boldsymbol{H} = 1$ T the average interval time is 60 s. Due to the discharging time of magnetic pulses in the millisecond range, the discharging time was often neglected when considering the magnetic field treatment time.

The Thermo Fisher-XRF was utilized to detect the major component of 2024 aluminum alloy. The X-350A type of x-ray stress meter was used to obtain the values of full width at half maximum (FWHM) so as to calculate the dislocation density. At this time the $\Psi$ angle was 0° and the normal diffractive crystal face was parallel to the normal sample surface. The

metallography observation was performed on the DYJ-905 inverted metallography microscope to obtain the morphology, size and distribution of precipitates in the alloy.

### 2.2. Theoretical calculation

In order to make clear the magnetic properties of main precipitates $\theta$ ($Al_2Cu$) in the alloy, the Materials Studio software (MS) was used to calculate the integrated spin density of state (DOS). At first, a three-dimensional (3D) structure model of the target phase was established on the basis of the first principle method. As for the first principles calculation, it was developed on the basis of the theory of quantum mechanics from the perspective of electronic structure evolution.[9] During the calculation, the density functional was the main theory to calculate the DOS of electrons so as to describe the system energy. In the present paper, the CASTEP software package,[10] based on the density functional theory, the lattice structure and the magnetic properties of $Al_2Cu$ were calculated and discussed in detail, providing some theoretical basis to explain the effect of the magnetic field, which is called the magneto plasticity effect.

## 3. Results and discussion

### 3.1. Tensile properties

In the process of magnetic field treatment, the $\boldsymbol{H}$ is one of the two important parameters to influence the tensile strength and elongation of 2024 aluminum alloy. From the experimental results of tensile properties at different values of $\boldsymbol{H}$, with 30 pulses fixed, the average tensile strength ($\sigma_b$) of 0.5 T, 1 T, 3 T, 5 T samples is 411 MPa, which is increased by 9.6% compared with the 375 MPa of an untreated sample. The elongation is 13.9% ($\delta$) on average, which is enhanced by 6.9% in comparison to the 13.0($\delta$) of an untreated sample.

Figure 2 demonstrates the tensile properties at different values of $\boldsymbol{H}$ (0.5 T, 1 T, 3 T, 5 T). It reveals that the tensile strength will increase with $\boldsymbol{H}$ enhancement. But it is not the case with the elongation tendency. When $\boldsymbol{H}$ increases from $0 \rightarrow 0.5$ T $\rightarrow 1$ T, the elongation increases gradually with $\boldsymbol{H}$ augment; while $\boldsymbol{H}$ increases from 1 T $\rightarrow$ 3 T $\rightarrow$ 5 T, the elongation exhibits a downtrend. In the range of $\boldsymbol{H} \leq 1$ T, the tensile strength and elongation of the alloy are improved synchronously in the presence of the magnetic field. Especially at $\boldsymbol{H} = 1$ T, the tensile strength and elongation are 410 MPa and 17.0% ($\delta$), and the amplifications are 9.3% and 30.8% respectively in comparison to the untreated sample. Therefore, it is regarded that 1 T is an optimized magnetic induction intensity as marked by $\boldsymbol{H}^*$.

In Fig. 3 the variation tendencies of tensile strength and elongation with the number of pulses increasing are presented. Based on the available information in Fig. 3, the effect of pulse number on the mechanical property can be summarized as follows. All the tensile strength ($\sigma_b$) of the magnetic field (MF) treated is enhanced in comparison to that of the untreated sample. The average $\sigma_b$ is 411 MPa, which is increased by 9.5% compared with that of the untreated sample. The average elongation is 15.3% ($\delta$) whose increment is 17.7%. In the whole processing, the magnetic field is beneficial to the synchronous increase of mechanical properties of alloys. Especially at $N = 30$, the elongation arrives at the 17% ($\delta$), amplified by 30.8%. Meanwhile the relevant tensile strength is 410 MPa that is 9.3% higher than that of the untreated sample. Hence, in order to maximize the effect of magnetic field the number of pulses, 30, is a suitable parameter and marked as $N^*$.

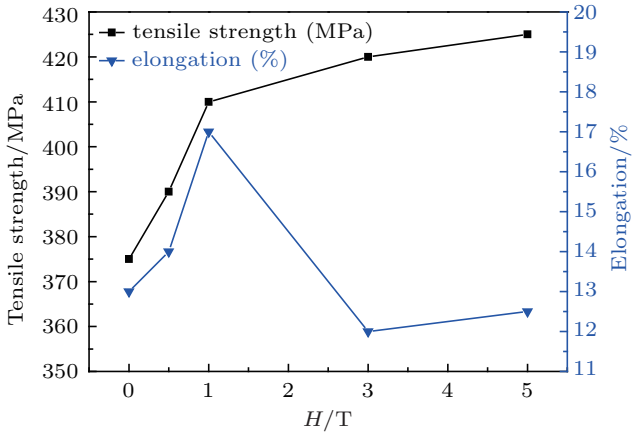



**Fig. 2.** (color online) Effects of $\boldsymbol{H}$ on the tensile strength and elongation of 2024 aluminum alloy.

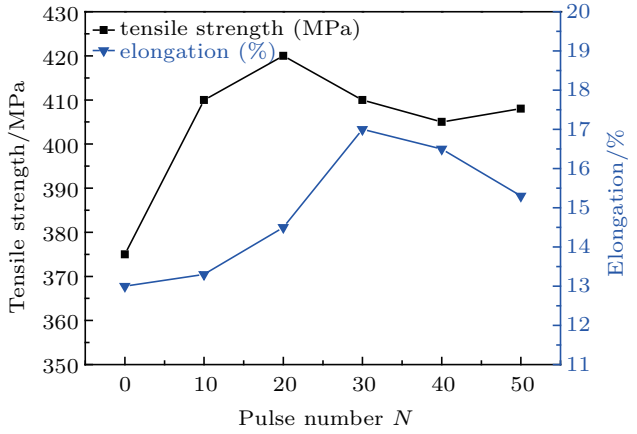



**Fig. 3.** (color online) Effects of $N$ on the tensile strength and elongation of 2024 aluminum alloy.

### 3.2. Action mechanism of magnetic field

From the above results we can conclude that the magnetic field has a great effect on the plasticity of alloy. Finding the main reason for activating the dislocation mobility and improving the plasticity of materials should be the first key issue to elucidate the experimental phenomenon.

According to the Faraday law of electromagnetic induction, the metallic sample placed in the solenoid coil electrified

by alternate current will induce an electric current. The electrified sample will be forced by the magnetic field, which is called the Lorentz force. The magnetic pressure $\boldsymbol{P}$ (in unit: MPa) imposed on the sample can be calculated from

$$\boldsymbol{P} = \frac{\boldsymbol{H}^2}{2\mu_0}, \tag{1}$$

where $\mu_0$ is the vacuum magnetic permeability of $4\pi \times 10^{-7}$ H/m,[11,12] when $\boldsymbol{H}^* = 1$ T, the calculated $\boldsymbol{P}$ is only 3.98 MPa, which is far less than the yield strength of conventional aluminum alloy. Hence, the Lorentz force generated by magnetic field is not enough to produce an extensive plastic deformation in aluminum alloy. On the other hand, for 2024 aluminum alloy, as a paramagnetic material, the magnetization force induced by the magnetic field is not yet reasonable for the extensive plastic deformation.

In view of the possible heat increase of the sample due to the pulsed magnetic field, the surface temperature of the sample was measured through hand touch and radiant thermometer. The test results show that after 30-pulse treatment, the surface temperature of the sample reaches about 30 °C∼40 °C on average, which is far away from the aging temperature and exhibits little influence on the microstructure and property of the sample. In fact, if the sample temperature increases to some extent, the elongation may therefore be enhanced, and the tensile strength will surely be lowered down. From Fig. 3 it can be seen that all the tensile strengths of MF treated samples increase compared with that of the untreated one. Hence, the possible effect of temperature increment due to magnetic field can be overlooked. From the characteristic of apparatus, the phenomenon is attributed to a low consuming power of the specially designed pulsed magnetic generator and a short duration of Joule heat induction.

The only reason to account for the phenomenon is deduced as the magneto plasticity effect (MPE).[13,14] The plasticity of 2024 aluminum crystals containing a large number of precipitates (acting as obstacles to the moving dislocations) is controlled by the pinning and depinning of dislocations from obstacles. The start of a dislocation motion is controlled by its freeing from obstacles. This becomes reasonable under the action of a strong enough mechanical stress. When the tensile test is performed under magnetic field, the influence of magnetic field on the dislocation, namely, the MPE should be taken into consideration.

In the nonmagnetic materials, such as 2024 aluminum alloy, there are a number of paramagnetic substances including dislocations and precipitates. The dislocations exhibit the paramagnetic property because of there being lots of electrons in them. In the 2024 aluminum alloy, the main precipitate is $\theta$ ($Al_2Cu$), whose paramagnetic property is calculated and demonstrated in the subsequent part. The magnitude of $\theta$ phase often acts as an obstacle for dislocation movement. For the paramagnetic dislocation or precipitates, in the absence of a magnetic field both the electron spin and the atomic intrinsic magnetic moment are in the disordered state; while in the presence of a high magnetic field their behaviors will be influenced apparently. During the tensile test under a magnetic field, when the active dislocations move close to the paramagnetic obstacles, the free electrons will be stimulated between the paramagnetic dislocations and obstacles, which contributes to form radical pairs just as shown in Fig. 4. In view of the differences in the spin combination of electron pairs, the radical pairs can be divided into four states, i.e., S, $T_0$, $T_+$, and $T_-$, which are shown in Figs. 5(e) and 5(f).

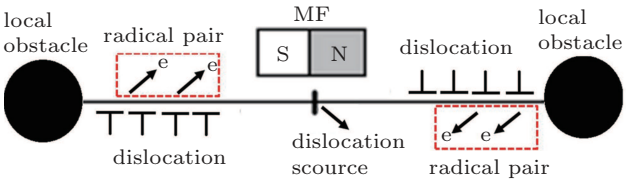



**Fig. 4.** (color online) Schematic diagram for free electron stimulation between the dislocation and obstacle.

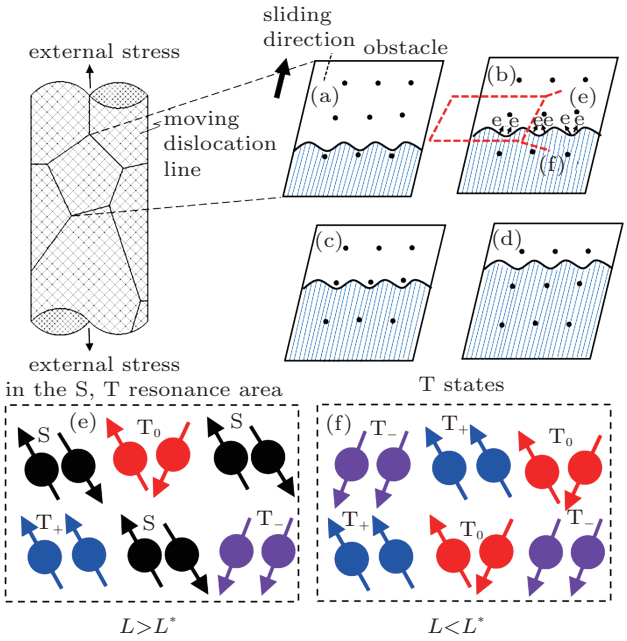



**Fig. 5.** (color online) Schematics of dislocation movement in the presence of a magnetic field. Panel (a) shows surmounting the previous obstacle and moving forward; panel (b) displays the motions close to the obstacles, in the cases of $L > L^*$ (e) and $L < L^*$ (f), with $L$ being the distance between dislocation and obstacles, and $L^*$ the critical one; panel (c) refers to the stay at the obstacles; panel (d) indicates the surmounting the obstacles and moving forward.

In the absence of a magnetic field, the radical pair is at the S state. For S state, the spin directions of electrons pair are opposite and the spin magnetic moments will be counteracted. On this condition, the energy required for dislocation to surmount obstacles is high.[15] The dislocation mobility decreases, therefore, elongation will be confined. When the sample is exposed to MF the spins of electron pairs will be influenced by the magnetic field and transform to the $T_0$, $T_+$ or

$T_-$ states. For the dislocations with T structural state the demanded energy will be lowered. Hence, it is easier for dislocations to move and surmount obstacles. At a macro level, for magnetic field treated 2024 aluminum alloy, it will induce a greater increase of elongation.

Figure 5 illustrates the schematic of dislocation movement in one period in the presences of magnetic field and external stress. Here, the parallelogram plane represents the sliding and the shadow refers to the region that has slid.

The whole process can be divided into four main steps as Figs. 5(a)–5(d).

Figure 5(a) (**Step 1**) shows the initial state of dislocation. Under the condition of external stress, the dislocation is free from the obstacles and moves forward along the sliding direction indicated by the black arrow. The demanded characteristic time is $10^{-3}$ s–$10^{-8}$ s. The accurate time is determined by the distance ($L$) between the moving dislocation and obstacles.

**Step 2** is the most complicated one in the whole process, which is displayed by Figs. 5(b), 5(e), and 5(f). During this period, the dislocation approaches to the next obstacle. The relationship between the dislocation and obstacle is determined by $L$, which is relevant to the radical pair state. When the $L$ is larger than $L^*$ (about $10^{-9}$ m) that is the critical length to distinguish the state of radical pair, the moving dislocation will pass through the S, T resonance area where the electron spin directions are random (Fig. 5(e)). In the presence of magnetic field, when the $L$ is smaller than $L^*$, the free electrons will be stimulated between the dislocation and obstacle (Fig. 5(b)) and two of them will generate a new radical pair. The time required to form a radical pair is $10^{-14}$ s$\sim$$10^{-6}$ s. The transitory time implies that the free electron stimulation and radical pair formation can be completed in the instantaneous time. The corresponding energy change $E_{\mathrm{M}}$ during the transition from the S to the $T_0$ state of the free radical pair can be calculated from

$$E_{\mathrm{M}} = \frac{1}{2}\Delta g \mu_{\mathrm{B}} H, \tag{2}$$

where $\Delta g$ is the difference in $g$ factor between radical pair states.[16]

Under the $\Delta g$ mechanism,[17] the radical pair lifetime ($\tau_{\mathrm{RP}}$) and the escape radical yield ($Y$) are influenced by an external magnetic field. The $\tau_{\mathrm{RP}}$ and $Y$ values from a triplet precursor should decrease with increasing magnetic field ($\boldsymbol{H}$) because the $T_0$–S spin conversion rate increases with increasing $\boldsymbol{H}$. Excluding the very weak magnetic field (hundreds Oe, 1 Oe = 79.5775 A·m$^{-1}$) the inter-combination transition is caused mainly by the difference in Zeeman frequency between electronic states forming the radical pair. That is to say, the radical pairs were impelled to transform from S state to $T_0$ by an external magnetic field.[18] Further the magnetic field will influence the electron spin and induce the atomic rearrangement, which directly results in the spin lattice relaxation. On this condition the radical pair will transit from $T_0$ to $T_+$, $T_-$ state (Fig. 5(f)).[19] The characteristic time for the atomic arrangement is in a range of $10^{-12}$ s–$10^{-8}$ s. In view of the energy difference, the S state of the radical pair implies a higher bonding energy between dislocation and obstacle when compared with an arbitrary state $T_0$, or $T_+$, or $T_-$. Therefore, a high coverage of radical pairs at the T state will contribute to the enhancement of plasticity of material, which can be achieved in the presence of a magnetic field. The experimental phenomenon is referred to as MPE. Apparently, the analysis and discussion about MPE is on a quantum scale.

As shown in Fig. 5(c) (**Step 3**), the dislocation is hindered and stays at the obstacles. Though the radical pair is at the T sate with lower bonding energy, the necessary impulsive energy is still needed. The possible energy resource comes from the stress or, sometimes, heat energy. The relevant characteristic time of this period ranges from $10^{-5}$ s to $\infty$. The symbol of "$\infty$" means that if there is not enough energy to stimulate the dislocation movement, the dislocation will stay at the obstacles for long.

In Fig. 5(d), when the critical demanded energy is absorbed, the dislocation will de-pin from the obstacle and move forward. The required time is $10^{-5}$ s–$10^{-10}$ s. Till now, one period of dislocation movement is terminated.

Comparing the characteristic times of the four steps, it can be concluded that the **Step 2** including the electron stimulation and atomic arrangement can end up in the momentary time, which meanwhile, demonstrates the high efficiency of magnetic field treatment. Nevertheless, **Step 3**, the stagnating and waiting of dislocations at obstacle location, is the most time-consuming period. It is regularly the rate-limiting step when performing the tensile test.

The previous research reveals that when the obstacles exhibit the paramagnetic properties, the MPE will perform efficiently.[5] In the following the electronic structure and the weak magnetic characteristic of the $\theta$ ($Al_2Cu$) phase are calculated and discussed. The cell structure of $\theta$ ($Al_2Cu$) belongs to a C16 square one with 12 atoms (eight Al and four Cu atoms). The lattice constants are $a = 0.6067$ nm and $b = 0.4877$ nm.[20]

Figure 6 shows the integrated density of spin states (integrated spin DOS) for $\theta$ that is calculated by the Materials Studio software.

At ground state the Fermi level is just the highest energy state for electrons. So the total integrated spin density of state of $Al_2Cu$ is below the ground state (Fig. 6(a)). When the integrated spin density of state from $-\infty$ to the Fermi level, the total integrated spin density of state can be acquired. As for

the electronic spin momentum $\mu$, it equals the product of total integrated spin density of state and $2\mu_B$ ($\mu_B$ is the Bohr magneton).[21] The calculated values of $\mu$ are listed in Table 2. It demonstrates that the spin magnetic moment of $Al_2Cu$ does not equal zero, so it is deduced as a paramagnetic property preliminarily.

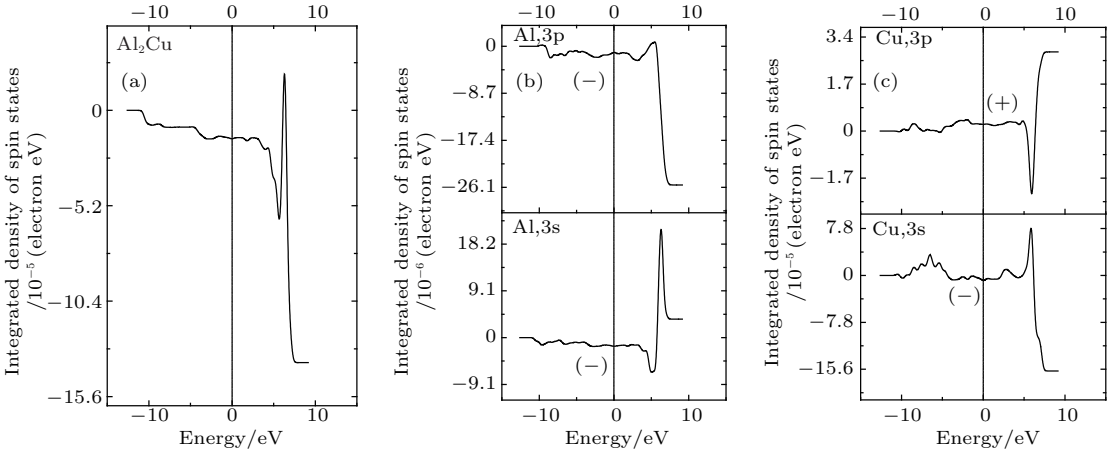



**Fig. 6.** Integrated spin DOS of $Al_2Cu$. (a) Total integrated spin DOS of $Al_2Cu$; (b) integrated spin DOS of Al 3s, 3p; (c) integrated spin DOS of Cu 3s, 3p.

**Table 2.** Calculated values of magnetic moment ($\mu$) of $Al_2Cu$ and relevant atoms.

| Magnetic moment | $\mu$ ($Al_2Cu$) | $\mu$ (Al) | $\mu$ (Cu) |
|---|---|---|---|
| Value | $-3.08\times10^{-5}$ $\mu_B$ | $-2.28\times10^{-6}$ $\mu_B$ | $4.88\times10^{-6}$ $\mu_B$ |

Next the electron configuration of different covalent bonds in $Al_2Cu$ should be analyzed in detail to further prove its magnetic performance. As shown in Fig. 6, at the position of Fermi level, the total spin direction of Al 3p (negative) is opposite to that of Cu 3p (positive), while the total spin direction of Al 3s orbit (negative) is identical to that of Cu 3s (negative). The same spin direction means that there are electrons with identical spin direction, namely, there exist unpaired electrons. As said by the Pauli principle of incompatibility, the minimum energy principle and the Hund rule, if there are unpaired electrons in the molecular orbit, it can be inferred that the molecule exhibits a paramagnetic property. Therefore, the $Al_2Cu$ molecule is deduced as a paramagnetic phase.

Further, the calculated valence states of Al and Cu atoms can be expressed by $[Ne](3s_f)^{0.4707}(3s_c)^{0.7648}(3p_c)^{1.7648}$ and $[Ar](4s_f)^{1.0}(4s_c)^{0.0}(4p_c)^{2.2752}(3d_c)^{2.2752}(3d_n)^{5.4496}$ separately where the subscripts "f " , "c" and "n" denote the free, covalent, and nonbonding electrons separately.[22] For example, the $3s_f$ and $3s_c$ are the free and covalent electron of 3s orbit. The $3p_c$ means the covalent electron of 3p orbit, and the $3d_c$ and $3d_n$ are the covalent and nonbonding electrons of 3d orbit respectively. The superscript indicates the relevant electron number. In the $Al_2Cu$ molecular orbit due to the existence of unpaired electrons, including free and nonbonding electrons the paramagnetic properties of the $Al_2Cu$ phase can be confirmed.

### 3.3. Dislocation characteristic

The plasticity is connected closely with the dislocation characteristics including its density, mobility and distribution.[23] The Dunn formula shown in formula (3) reveals the relationship between dislocation density $\rho$ and the full width of half maximum ($L$) in the x-ray diffractomer (XRD) pattern[24,25]

$$\rho = \frac{L^2}{4.35\times b^2}, \tag{3}$$

where $b$ is the Burgers vector.[26] From formula (3) it can be deduced that the dislocation density $\rho$ is proportional to $L^2$.

Figure 7 displays the relationship between $L^2$ and $\boldsymbol{H}$ ($N^*=30$). The variation tendency is similar to that of elongation (Fig. 2). The $L$ values of the samples subjected to different values of $\boldsymbol{H}$ are 0.3320, 0.3562, 0.3762, 0.2794, 0.3556, which correspond to the magnetic induction intensities 0 T, 0.5 T, 1 T, 3 T, and 5 T respectively. The values of relevant $L^2$ are 0.1102, 0.1269, 0.1415, 0.0781, and 0.1265, corresponding to 0 T, 0.5 T, 1 T, 3 T, and 5 T, respectively. The $L^2$ at $\boldsymbol{H}^*=1$ T is 1.28 times higher than that of the untreated sample.

Figure 8 shows the dependence of $L^2$ on pulse number $N$ ($\boldsymbol{H}^*=1$ T). It can be ascertained that the tendency is similar to that of elongation (Fig. 3). When $N^*=30$, the $L^2$ is 1.28 times higher than that of the untreated sample.

The relationships between $L^2$ and $\boldsymbol{H}$, $N$ have similar tendencies to those between the elongation and $\boldsymbol{H}$, $N$. The regularity is totally different from the conventional phenomenon as work hardening, namely, the more amounts of plastic deformation and dislocation density, the less elongation and plasticity. On the basis of previous analysis, we can know that in the presence of a magnetic field, the dislocation mobility has been enhanced due to the magnetic plasticity effect. Under the condition of $\boldsymbol{H}^*=1$ T and $N^*=30$, the effect of a high magnetic field arrives at an utmost state. Meanwhile, the dislocation mobility and flexibility turn better, which are beneficial to the dislocation proliferation and density increment.[27]

At the optimized magnetic field parameter, the proliferous dislocation will not be tangled and accumulated. Therefore, the work hardening will not take any effect.

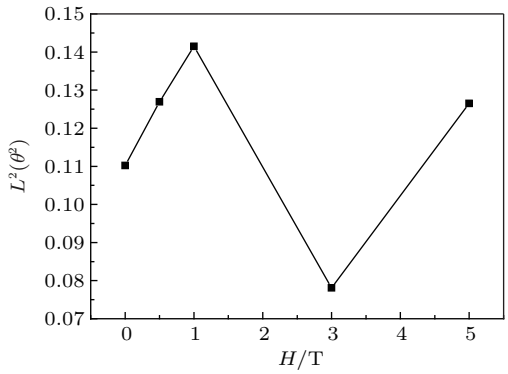



**Fig. 7.** Dependence of $L^2$ on the $\boldsymbol{H}$ when $N^* = 30$.

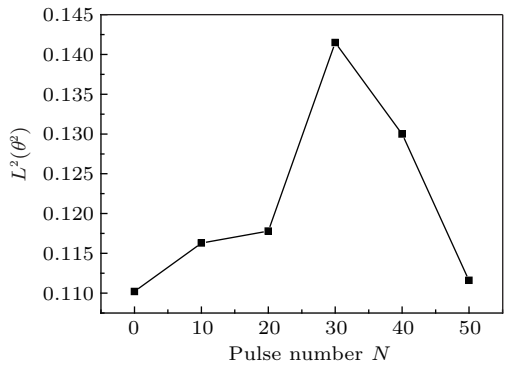



**Fig. 8.** Dependence of $L^2$ on $N$ when $\boldsymbol{H}^* = 1$ T.

However, when the dislocation density increases to a certain amount ($\boldsymbol{H}^* = 1$ T in Fig. 7 and $N^* = 30$ in Fig. 8), large numbers of dislocations may accumulate at the grain boundary and destroy the moving flexibility of dislocations, accompanied by the decrease of plasticity. It often induces the dynamic recrystallization with the tensile test processing together with the grain refinement and preferred orientation, which will be explained later. This will consume the dislocation amount and result in the decrease of dislocation density.

### 3.4. Grain size

The grain sizes of the sample acquired by the XRD test are illustrated in Table 3.

**Table 3.** Grain sizes of samples subjected to different values of $\boldsymbol{H}$ and $N$.

| $\boldsymbol{H}$/T | $N$ | $d$/nm |
|---|---|---|
| 0 | 0 | 410.6 |
| 0.5 | 30 | 279.8 (↓31.9%) |
| 1 ($\boldsymbol{H}^*$) | 30 ($N^*$) | 266.1 (↓35.2%) |
| 3 | 30 | 444.0 |
| 5 | 30 | 273.8 (↓33.3%) |
| 1 | 10 | 295.4 (↓28.1%) |
| 1 | 20 | 333.8 (↓18.7%) |
| 1 ($\boldsymbol{H}^*$) | 30 ($N^*$) | 266.1 (↓35.2%) |
| 1 | 40 | 318.2 (↓22.5%) |
| 1 | 50 | 309.8 (↓24.5%) |

It can be seen that the grain size ($d$ in nm) is influenced by the magnetic field parameter. Especially under the condition of $\boldsymbol{H}^* = 1$ T and $N^* = 30$, the grain size acquires a minimum value of 266.1 nm, which is reduced by 35.2% compared with that of the untreated sample (410.6 nm).

It can be seen that the high pulsed magnetic field has a strong effect on grain refinement. The fine grains exhibit the fine grain strengthening and contribute to enhancing the strength and the plasticity of material synchronously. It is analyzed that the grain refinement is closely related to the evolution of dislocation density.

As shown in Figs. 7 and 8, under the condition of $\boldsymbol{H}^* = 1$ T and $N^* = 30$, the dislocation density arrives at an utmost. Some of them will accumulate and pile up at the grain boundary. The subsequent dynamic recrystallization will contribute to the grain refining that can be illustrated in Fig. 9. In the synchronous presence of a high magnetic field and external stress, the moving flexibility of dislocations will be enhanced (Fig. 9(a)). When more and more dislocations accumulate at the grain boundary, the stress concentration will take place at the tip of the leading dislocation (Fig. 9(b)). On this condition, the dislocations with opposite sign will counteract each other and form a dislocation network with low energy. The sub-grain boundary will be generated subsequently. With the dislocation moving further, the sub-grain boundary will connect with the surrounding grain boundary or sub-grain boundary, the result of which is the formation of fine sub-grains (Fig. 9(c)).[28]

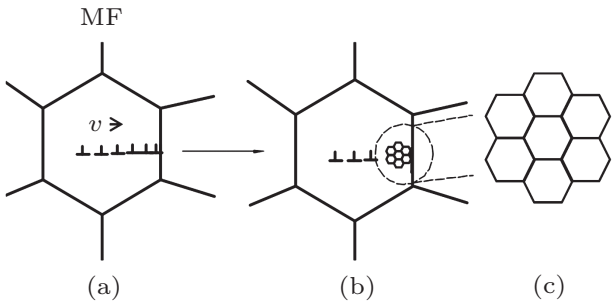



**Fig. 9.** Schematic diagram of dynamic recrystallization in the tensile process. (a) Dislocation accumulation at the grain boundary; (b) formation of fine sub-grains; (c) the enlarged fine grains.

### 3.5. Texture

Figure 10 shows the XRD patterns of samples with different values of $\boldsymbol{H}$ ($N^* = 30$). As for the $\boldsymbol{H}^* = 1$ T sample, when compared with the $\boldsymbol{H} = 0$ T one, the peak intensities of (211) and (220) are weakened and (411) strengthened. It highlights that the magnetic field has changed the texture of alloy towards the direction of plasticity improvement. At $\boldsymbol{H} = 3$ T and $\boldsymbol{H} = 5$ T, the crystal orientations do not change apparently at (211) and (220) except for a little increment of the (411) peak. It is concluded that when $\boldsymbol{H}$ is larger than 1 T, the effect of magnetic field on the texture will become weak.

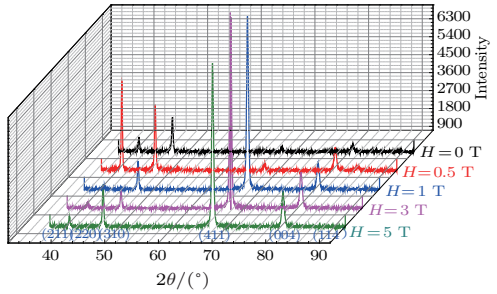



**Fig. 10.** (color online) Dependences of XRD pattern on the $\boldsymbol{H}$ when $N^* = 30$.

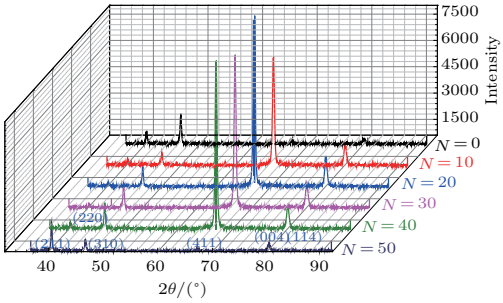



**Fig. 11.** (color online) Dependences of XRD diagram on the $N$ when $\boldsymbol{H}^* = 1$ T.

Figure 11 displays the XRD patterns at different $N$ values ($\boldsymbol{H}^* = 1$ T). At $N = 10$, 20, 30, 40, the XRD configuration has changed significantly in comparison with those of the $N = 0$ and $N = 50$ sample. Namely, the intensities of (211) and (220) peaks are weakened while the (411) and (004) peaks strengthened obviously. The phenomenon demonstrates that in the relevant magnetic field duration corresponding to the 10–40 pulse treatment, the crystal texture will be influenced apparently; while at $N = 50$, the effect of magnetic field tends to be at a statured state. That is to say, the texture of the $N = 50$ sample is similar to that of the $N = 0$ sample. The result is identical to the variation tendency in Fig. 8.

Table 4 lists the peak intensities of (211) and (220) crystal plane at different magnetic parameters. It can be seen that under the condition of $\boldsymbol{H}^* = 1$ T and $N^* = 30$, the peak intensities of (211) and (220) crystal planes are lower than those values under other magnetic parameters. It can be deduced that when the textures of (211) and (220) crystal planes are weakened, the elongation or plasticity will be much increased. The weakened texture contributes to the slipping of basal faces, and then the enhancing of plasticity.

**Table 4.** Peak intensities of (211) and (220) crystal plane with different values of $\boldsymbol{H}$ and $N$.

| $\boldsymbol{H}$/T | $N$ | (211) plane | (220) plane |
|---|---|---|---|
| 0 | 0 | 715 | 73 |
| 0.5 | 30 ($N^*$) | 4417 | 55 |
| 1 ($\boldsymbol{H}^*$) | 30 ($N^*$) | **183** | **35** |
| 3 | 30 ($N^*$) | 284 | 59 |
| 5 | 30 ($N^*$) | 504 | 49 |
| 1 ($\boldsymbol{H}^*$) | 10 | 268 | 50 |
| 1 ($\boldsymbol{H}^*$) | 20 | 246 | 52 |
| 1 ($\boldsymbol{H}^*$) | 30 ($N^*$) | **183** | **35** |
| 1 ($\boldsymbol{H}^*$) | 40 | 324 | 50 |
| 1 ($\boldsymbol{H}^*$) | 50 | 1585 | 34 |

The orientation effect of the magnetic field should be responsible for the texture weakening. As shown in Fig. 9, during the grain refinement, the orientation of newborn fine grains will rotate about the magnetic field. It is deduced that in the alloy with magnetic anisotropy characteristic, the magnetic susceptibility along the glide planes is higher than those in other planes. Therefore, when the tensile sample is exposed to the magnetic field, the texture along the non-glide plane, such as (211) and (200) will be weakened while that along the glide plane will be strengthened. Figure 12 illustrates the XRD pattern and the orientation schematics of crystal grains without and with MF.

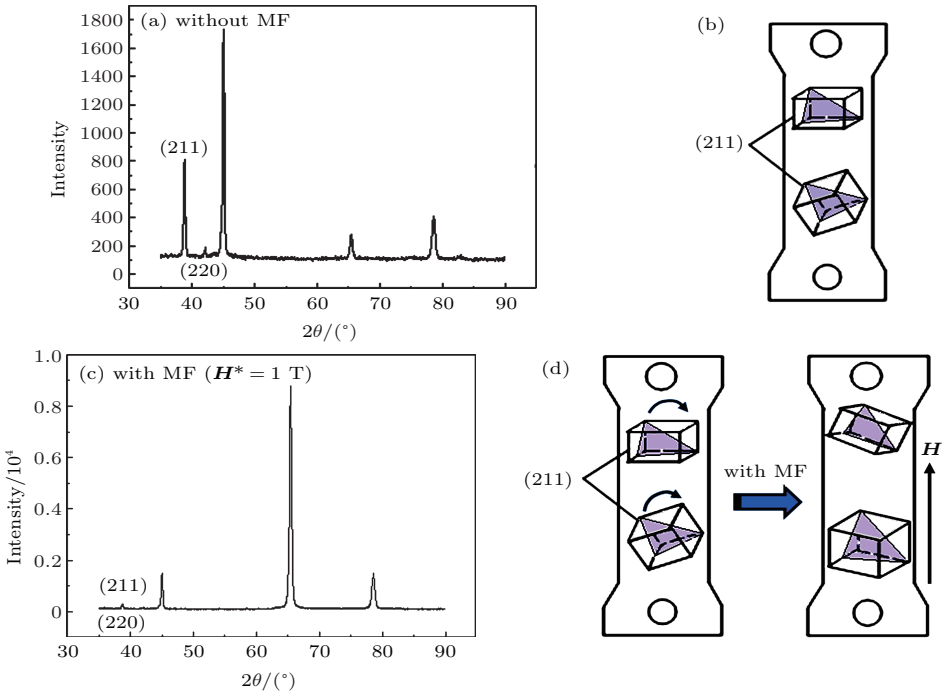



**Fig. 12.** (color online) XRD pattern and the orientations of crystal grains without and with magnetic field (MF). (a) XRD without MF; (b) the preferred orientation of (211) cardinal plane; (c) XRD with $\boldsymbol{H}^* = 1$ T MF; (d) crystal axis rotation in 1 T tensile sample.

## 4. Conclusions

The high magnetic field has an apparent effect on the tensile properties of 2024 alloy in the presences of both magnetic field and external stress. At $\boldsymbol{H}^* = 1$ T and $N^* = 30$, the tensile strength and elongation are increased synchronously by 9.3% and 30.8% in comparison to the untreated sample, respectively. The action mechanism of the magnetic field does not lie in the Lorentz force, nor magnetization force nor temperature, but the MPE. The magnetic field will accelerate the state conversion of a radical pair generated between the dislocation and precipitates (obstacles) from singlet to the triplet state, and the bonding energy between dislocation and obstacle will be lowered down. The moving flexibility of dislocations will be enhanced. On the basis of first principle, the magnetic property of main precipitate $\theta$ ($Al_2Cu$) is ascertained as paramagnetic, which is beneficial to the MPE exertion. At $\boldsymbol{H}^* = 1$ T and $N^* = 30$, when compared with that in the untreated sample, the dislocation density is enhanced by 1.28 times. The relevant minimum grain size is 266.1 nm, which is reduced by 35.2%. The grain refining is attributed to the dislocation accumulation and subsequent dynamic recrystallization. From the XRD pattern it can be seen that the (211) and (220) peak intensities are weakened. It is deduced that together with the recrystallization, the fined grains will transfer towards the slip plane and contribute to the slipping deformation.

## References


[1] Tolga Dursun and Costas Soutis 2014 *Materials and Design* **56** 862

[2] Shahsavaria, F. Karimzadeha, A. Rezaeiana and H. Heydaria 2015 *Procedia Materials Science* **11** 84

[3] Benachour M, Hadjoui A, Benguediab M and Benachour N 2010 *Procedia Engineering* **02** 121

[4] Asai S 2000 *Sci. Technol. Adv. Mater.* **01** 191

[5] Wang C J, Wang Q, Wang Y Q, Huang J and He J C 2006 *Acta Phys. Sin.* **55** 2 (in Chinese)

[6] Rao X J, Zhong Y B, Zhang Z G, Wang Z Q, Deng K, Ren Z M and Xu K D 2012 *Acta Phys. Sin.* **61** 221301 (in Chinese)

[7] Katsuyuki Kida, Masayuki Ishida, Mika Furuse, Koshiro Mizobe and Edson Costa Santos 2016 *International Journal of Fatigue* **88** 156

[8] Li G R, Li Y M, Wang F F and Wang H M 2015 *Chinese Journal of Nonferrous Metals* **25** 331 (in Chinese)

[9] Lalic M V and Souza S O 2008 *Opt. Mater.* **30** 1189

[10] Kohn W and Sham L J 1965 *Phys. Rev. A* **140** 1133

[11] Li G R, Zhao Y T and Dai Q X 2007 *Journal of University of Science and Technology Beijing, Mineral, Metallurgy, Material* **14** 460

[12] Wang H M, Li P S, Zhen R, Li G R and Yuan X T 2015 *Acta Phys. Sin.* **64** 087104 (in Chinese)

[13] Golovin Y I 2004 *Phys. Solid State* **46** 789

[14] Alshits V I, Darinskaya E V, Kazakova O L, Mikhina E Yu and Petrzhik E A 1997 *Mater. Sci. Eng. A* **234–236** 617

[15] Molotskii M I and Fleurov V J 2000 *Phys. Chem. B* **104** 3812

[16] Li G R, Wang H M, Li P S, Gao L Z, Peng Z X and Zhen R 2015 *Acta Phys. Sin.* **64** 148102 (in Chinese)

[17] Salikhov K M, Molin Yu N, Sagdeev R Z and Buchachenko A L 1984 *Spin Polarization and Magnetic Effects in Radical Reactions* (Amsterdam: Elsevier)

[18] Molotskii M and Fleurov V 1997 *Phys. Rev. Lett.* **78** 2779

[19] Ashby M F and Johnson K L 2006 *Philos. Mag. A* **20** 1009

[20] Gao Y J and Huang C G 2004 *Func. Mater.* **35** 1103 (in Chinese)

[21] Wang H M, Zhen R and Li G R 2015 *Chinese Journal of Inorganic Chemistry* **31** 2143 (in Chinese)

[22] Huang C G, Wen C L, Wei N, Liu H and Gao Y J 2010 *Non-ferrous Metals* **62** 01 (in Chinese)

[23] Liu Z L, Hu H Y and Fan T Y 2007 *Journal of Beijing Institute of Technology* **27** 113

[24] Cai Y Q, Sun J Z, Liu C J, Ma S W and Wei X C 2015 *Journal of Iron and Steel Research* **22** 1024

[25] Korznikov A V, Safarov I M, Nazarov A A and Valiev R Z 1996 *Mater. Sci. Eng. A* **206** 39

[26] Zhang J C, Wang J F, Wang Y T and Yang H 2004 *J. Phys.* **8** 2468

[27] Ni S, Wang Y B, Liao X Z, Figueiredob R B and Li H J 2012 *Acta Mater.* **60** 3181

[28] Liu P and Chen Z J 2011 *Journal of Hefei University of Technology (Natural Edition)* **34** 341 (in Chinese)